arXiv:1406.1750v3 [cond-mat.stat-mech] 16 Jan 2015

First-order directional ordering transition in the three-dimensional compass model

Max H. Gerlach[1,2,*] and Wolfhard Janke[1,†]

[1]*Institut für Theoretische Physik and Centre for Theoretical Sciences (NTZ), Universität Leipzig, Postfach 100 920, 04009 Leipzig, Germany*

[2]*Institut für Theoretische Physik, Universität zu Köln, Zülpicher Str. 77, 50937 Köln, Germany*

(Dated: January 19, 2015)

We study the low-temperature properties of the classical three-dimensional compass or t_{2g} orbital model on simple-cubic lattices by means of comprehensive large-scale Monte Carlo simulations. Our numerical results give evidence for a directionally ordered phase that is reached via a first-order transition at the temperature $T_0 = 0.098328(3)J/k_B$. To obtain our results we employ local and cluster update algorithms, parallel tempering and multiple histogram reweighting as well as model-specific screw-periodic boundary conditions, which help counteract severe finite-size effects.

PACS numbers: 05.70.Fh, 75.10.Hk, 75.40.Mg

I. INTRODUCTION

The compass model[1] is a generic model for orbital-orbital interactions in certain Mott insulators such as various transition-metal compounds. In systems with partially filled orbital $3d$ shells it provides a heuristic description for the coupling of t_{2g} orbitals. If their interaction is dominated by the Kugel-Khomskii superexchange mechanism, the quantum compass model is realized, while the phonon-mediated Jahn-Teller effect gives rise to the classical compass model.[2,3] Beyond the rich physics of orbital order in recent years the quantum compass model has received increased attention because it provides an alternative route to realize qubits that are shielded from decoherence via so-called topological protection.[4,5] In this context the model is realized in the form of arrays of superconducting Josephson junctions, which have already been implemented successfully in experiments.[6]

While the compass model is closely related to the well-studied $O(n)$ and Heisenberg lattice spin models with nearest-neighbor interactions, it differs from these in a fundamental aspect: It features an inherent coupling of real space symmetry, realized by the point group of the lattice, to the symmetry of the interactions encoded in the Hamiltonian. The resulting competition of exchange couplings along the different lattice axes prevents a conventional magnetization-like ordered phase, but still allows for long-ranged, essentially one-dimensional directional ordering.[7] The peculiar symmetries of the compass model lead to a high degree of degeneracy in its ground states,[8] similarly to other orbital models.[1] Typically such a degeneracy suppresses order for $T = 0$, while at low, but finite temperatures an ordered phase may still be realized through an order-by-disorder[9,10] mechanism, where certain system configurations are favored entropically. For both the classical and the quantum variation of the compass model in two dimensions (2D), earlier Monte Carlo studies have indeed established the realization of a directionally ordered phase at low temperatures, which is reached by a continuous thermal phase transition in the 2D Ising universality class.[11–13]

Beyond that, the case of the three-dimensional (3D) compass model remains particularly interesting as it may be significant for the microscopic description of materials in the reach of experimental research. For the 3D quantum compass model high-temperature series expansions have not shown any sign of a finite-temperature phase transition, while the continuous transition could be confirmed for the 2D quantum compass model.[14]

The purpose of this paper is to shed more light on the low-temperature properties of the compass model in three dimensions. We present an extensive Monte Carlo study that provides evidence for a first-order phase transition from a high-temperature disordered phase into a directionally ordered phase. While simulations of the quantum model are plagued by a negative-sign problem and hence are infeasible on reasonably sized lattices, we can study the classical variation of the 3D compass model without prohibitive computational cost. Nevertheless, a considerable methodological effort is required to obtain quantitative results for two reasons: The model features very strong finite-size effects that must be treated carefully and long autocorrelation times near the transition point would make it hard to collect sufficient statistics with only a naive Monte Carlo sampling scheme.

The main part of this work is organized as follows: In Sec. II we formally introduce the model and discuss some of its properties. Section III describes the setup of the simulations and the specific numerical methods employed. Our results are presented and analyzed in Sec. IV. We close in Sec. V with conclusions and an outlook.

II. THE MODEL

In d spatial dimensions the compass model is defined on a simple-hypercubic lattice of size $N = L^d$ by the Hamiltonian

$$\mathcal{H} = -\sum_{k=1}^{d}\sum_{i=1}^{N} J_k s_i^k s_{i+\hat{\mathbf{k}}}^k. \tag{1}$$

Here s_i^k is the k-th component of a spin $\mathbf{s}_i$ at lattice site i. J_k is a coupling constant depending on the lattice direction k. The nearest neighbor of site i in the k-th direction is indicated by $i + \hat{\mathbf{k}}$. In the classical compass model the constituent spins are represented by vectors on the unit hypersphere in d-dimensional space: $\mathbf{s}_i \in S^{d-1}$. Two spins on sites neighboring in direction k only interact in their k-th components.

Note that Eq. (1) could be separated into d independent one-dimensional Hamiltonians, if the directions were not coupled by the constraint $|\mathbf{s}_i| = 1$.

In this paper we limit the discussion to equal coupling constants in every direction: $J_k \equiv J$. The Hamiltonian of the three-dimensional model on a cubic lattice of size $N = L^3$ then reads

$$\mathcal{H}^{(3D)} = -J \sum_{i=1}^{N} \left[s_i^x s_{i+\hat{\mathbf{x}}}^x + s_i^y s_{i+\hat{\mathbf{y}}}^y + s_i^z s_{i+\hat{\mathbf{z}}}^z \right], \tag{2}$$

where the spins $\mathbf{s}_i \in S^2$ can be parametrized by azimuthal and polar angles $\theta_i \in [0, \pi]$ and $\varphi_i \in [0, 2\pi)$:

$$\mathbf{s}_i = \mathbf{s}(\theta_i, \varphi_i) = \begin{pmatrix} s_i^x \\ s_i^y \\ s_i^z \end{pmatrix} = \begin{pmatrix} \sin\theta_i \cos\varphi_i \\ \sin\theta_i \sin\varphi_i \\ \cos\theta_i \end{pmatrix}. \tag{3}$$

In this work we choose a coupling constant of $J > 0$ corresponding to ferromagnetic interactions.

The classical compass model is obtained by taking the limit of large spin S of the quantum mechanical compass model, where the spins would be represented by $S = 1/2$ operators $\mathbf{s}_i = \frac{\hbar}{2}(\sigma_x, \sigma_y, \sigma_z)$ with the Pauli matrices σ_k.

The compass model in Eq. (1) has a high number of ground states. To begin with, any constant spin configuration is a ground state. Beyond that, the model exhibits a number of discrete symmetries, which lead to a macroscopic degeneracy of every energetic state, including but not limited to the ground state.[1,8] Most importantly for $d = 3$ with open or periodic boundary conditions, Eq. (2) is invariant under a reflection of all spins on any line of sites parallel to one of the lattice axes across the orthogonal plane, which leads to a 2^{3L^2}-fold degeneracy. As a consequence of these gauge-like symmetries conventional magnetic order is prohibited at any temperature:[7] $\langle m \rangle = \langle |\frac{1}{N} \sum_i \mathbf{s}_i| \rangle \equiv 0$. However, quantities such as $\langle s_i^k s_{i+\hat{\mathbf{k}}}^k \rangle$ are invariant under these symmetries and a special type of directional or "nematic" ordering is not precluded. One can construct order parameters that measure directional ordering characterized by long-rang correlations in the direction of fluctuations in spin and lattice spaces, even though magnetic ordering is absent. This type of order is realized by linear spin alignment parallel to the lattice axes so that nearest-neighbor bonds carrying the lowest energy are oriented mostly along one specific direction as illustrated in Fig. 1. It is not obvious to which degree the ground-state degeneracy translates into the number of distinct directionally ordered phases at low finite temperature.

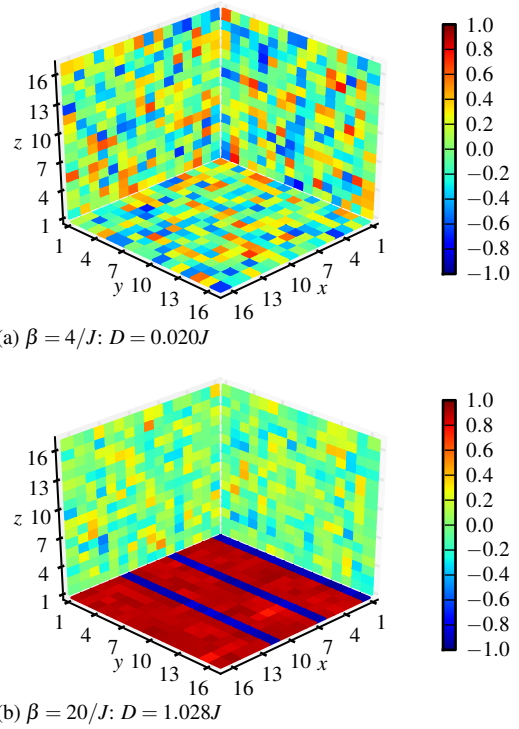

(a) $\beta = 4/J$: $D = 0.020J$

(b) $\beta = 20/J$: $D = 1.028J$

FIG. 1. (Color online) Shown are two typical example spin configurations of the $L = 16$ system from (a) the disordered high-temperature phase and (b) the directionally ordered low-temperature phase. On each face of the cube the averaged projection to the orthogonal direction of all spins at sites in one column above that face is given color-coded. While in the high-temperature snapshot at $\beta = 4/J$ no order can be recognized, there is a strong tendency towards linear alignment of the spins in the $\pm\hat{\mathbf{z}}$-directions in the low-temperature snapshot at $\beta = 20/J$.

III. NUMERICAL METHODS

A. Observables

We now turn to our numerical simulations of Eq. (2) carried out at various inverse temperatures $\beta = 1/k_B T$ and first discuss the quantities we measure. By $E_k = -J \sum_{i=1}^{N} s_i^k s_{i+\hat{\mathbf{k}}}^k$ with $k = x, y, z$ we denote the total bond energy along the k-th lattice axis. Our basic observable is then the total energy

$$E = E_x + E_y + E_z \tag{4}$$

with the corresponding heat capacity

$$C = \frac{\partial E}{\partial T} = k_B \beta^2 \left[\langle E^2 \rangle - \langle E \rangle^2 \right]. \tag{5}$$

In previous studies an order parameter for directional ordering in the two-dimensional model has been defined by the energy excess in one of the lattice directions compared to the other direction.[11–13] Here we consider a three-dimensional extension

$$D = \frac{1}{N} \sqrt{(E_y - E_x)^2 + (E_z - E_y)^2 + (E_x - E_z)^2}. \tag{6}$$

To help with the analysis of the directional ordering phase transition and its finite-size scaling we also consider quantities derived from D: the susceptibility χ and the Binder parameter Q_2, which are defined as

$$\chi = N \left[\langle D^2 \rangle - \langle D \rangle^2 \right], \qquad Q_2 = 1 - \frac{1}{3} \frac{\langle D^4 \rangle}{\langle D^2 \rangle^2}. \tag{7}$$

B. Screw-periodic boundary conditions

In most cases simulations of statistical models are carried out on finite lattices with the topology of a torus, i.e., with periodic boundary conditions. The assumption is that compared to open or fixed boundary conditions this choice minimizes finite-size surface effects, which become irrelevant in the thermodynamic limit.

In previous studies of the two-dimensional classical compass model, however, periodic boundary conditions have not turned out to be an ideal choice. In the directionally ordered low-temperature phase the spins form essentially one-dimensional chains with decoupled rows and columns of spins on the square lattice. With periodic boundary conditions the spins tend to form closed aligned loops along the boundaries of a finite lattice. Such excitations are particularly stable against thermal fluctuations. In their studies Mishra et al. have noticed such an effect spoiling the finite-size scaling with periodic boundary conditions[11] and suggested that the reason may lie in the existence of a one-dimensional magnetic correlation length ξ_{1D} which exceeds the linear system size L at low temperatures. Wenzel et al. have confirmed this claim.[13]

As a solution the authors of Ref. 11 have adopted special fluctuating or annealed boundary conditions. Here the signs of the coupling constants on the bonds at the lattice boundaries are allowed to fluctuate thermally. In this way, one-dimensional chains are effectively broken up. While one can assume that the influence of these dL^{d-1} fluctuating bonds becomes unimportant in the thermodynamic limit as $N = L^d \to \infty$, this choice still constitutes a considerable modification of the model and no good finite-size scaling theory is available for this type of boundary conditions.

As an alternative the authors of Ref. 13 have proposed screw-periodic boundary conditions, which are a particular deformation of the torus topology of regular periodic boundary conditions. We generalize their definition to three dimensions to obtain boundary conditions that interconnect lines of spins along any of the principal lattice directions. Explicitly, the nearest neighbors of a site $i = (x, y, z)$ in directions $\hat{\mathbf{x}}$, $\hat{\mathbf{y}}$, $\hat{\mathbf{z}}$ are specified as follows:

$$
\begin{aligned}
(x,y,z)+\hat{\mathbf{x}} &= \begin{cases} (x+1,y,z), & \text{if } x < L-1, \\ (0,y,[z+S] \bmod L), & \text{if } x = L-1, \end{cases} \\
(x,y,z)+\hat{\mathbf{y}} &= \begin{cases} (x,y+1,z), & \text{if } y < L-1, \\ ([x+S] \bmod L,0,z), & \text{if } y = L-1, \end{cases} \\
(x,y,z)+\hat{\mathbf{z}} &= \begin{cases} (x,y,z+1), & \text{if } z < L-1, \\ (x,[y+S] \bmod L,0), & \text{if } z = L-1. \end{cases}
\end{aligned}
\tag{8}
$$

Here the screw length S is a parameter that can be varied. If S is taken as one of the distinct divisors of L, each plane of the lattice can be subdivided into S groups of sites or "loops" in each in-plane direction $\hat{\mathbf{k}}$, which are linked as pairs of neighbors along that direction. With $S = 0$ or $S = L$ regular periodic boundary conditions are recovered. With $S = 1$ there are only single loops for each direction in a plane. The power of screw-periodic boundary conditions lies in the fact that with a sufficiently low choice of S, the loop length exceeds the magnetic correlation length ξ_{1D} already for small L. Hence, linearly aligned excitations are broken up more easily than with regular periodic boundary conditions. Besides that the screw-periodic boundary conditions reduce the number of discrete symmetries in the compass model and the energetic degeneracy of its configurations such that the leading degeneracy factor mentioned at the end of Sec. II is lowered from 2^{3L^2} to 2^{3L}.

We have found that also for the three-dimensional model regular periodic boundary conditions lead to poor finite-size scaling results. Moreover, the simple definition (6) of the order parameter D is disadvantageous with these boundary conditions because it assigns different values to configurations which differ by planar rotations, but really show an equal degree of order. To remedy both problems we use screw-periodic boundary conditions according to the definition (8) with a choice of $S = 1$.

The choice of these boundary conditions is not expected to have an influence on the thermodynamic limit. They have also been successfully applied for other purposes, e.g., for the controlled formation of tilted interfaces between ordered domains in the Ising model.[15]

C. Monte Carlo methods

In the following section we outline the Monte Carlo algorithms applied in our simulations.

Fundamentally we use the standard Metropolis algorithm[16] for local single-spin updates. In one lattice sweep new orientations are proposed in sequential order for the spins at all sites. The direction of the new spin vector is chosen randomly from a uniform distribution over the surface area of a spherical cap centered around the original vector. To ensure proper uniform sampling of the angular variables the spherical measure of integration $\sin\theta\, d\theta\, d\varphi$ is respected. During thermalization we adjust the opening angle of this spherical cap in such a way that an average acceptance ratio of 50% is realized at each temperature.

To reduce autocorrelation times we additionally use the one-dimensional version of the Wolff cluster update[17] introduced earlier for the 2D compass model[13] in a direct extension to the 3D model. This update exploits one of the discrete symmetries of the Hamiltonian, which is left invariant if a line of neighboring spins along one of the lattice directions is reflected about the plane orthogonal to that direction. To construct a cluster first a random starting site i and a lattice direction $\hat{\mathbf{k}} \in \{\hat{\mathbf{x}}, \hat{\mathbf{y}}, \hat{\mathbf{z}}\}$ are chosen and the spin $s_i^k \to -s_i^k$ is flipped, then neighboring sites in directions $\pm\hat{\mathbf{k}}$ are added to the cluster with probability

$$
P_{i,i\pm\hat{\mathbf{k}}}(\mathbf{s}_i, \mathbf{s}_{i\pm\hat{\mathbf{k}}}) = 1 - \exp\left(\min\left\{0, 2\beta J s_i^k s_{i\pm\hat{\mathbf{k}}}^k\right\}\right). \tag{9}
$$

This step is iterated with the newly adjoined site $i \pm \hat{\mathbf{k}}$ taking the place of i until no further sites are added. All spins in the strictly one-dimensional cluster constructed in this way are thus flipped at the same time. Due to the restricted set

of possible reflection planes, this update is not ergodic on its own, but must be used in combination with local spin updates. In our simulations $3L$ cluster updates in randomly chosen directions are followed by $N = L^3$ local updates and we count this combination as one Monte Carlo sweep.

To further reduce autocorrelation times and improve statistics we combine these canonical algorithms with a parallel-tempering scheme.[18,19] Different replicas of the system are simulated simultaneously at various inverse temperatures β_k. We propose exchanges of system configurations between replicas at adjunct temperature points every 100 sweeps. The range of simulation temperatures is chosen according to the scheme of constant entropy increase,[20] which clusters the temperature points close to a phase transition and thus eases diffusion in temperature space, which has been valuable for the simulations on large lattices.

From the measurements taken in the various replicas we obtain time series of the observables D and E at various discrete inverse temperatures β_k. Making use of multiple histogram reweighting techniques[21] these observables as well as the derived quantities χ, Q_2 and C can be estimated also at arbitrary intermediate temperatures from the optimally combined simulation data. We limit discretization errors by computing per-sample weighting factors from the density of states and reweighting observable time series directly.[22] By applying Brent's algorithm for minimization[23] we can precisely determine extremal temperature locations and values of χ, Q_2 and C or other quantities which are useful to characterize the finite-size scaling behavior at a phase transition. Estimates of the statistical uncertainties of these quantities are obtained by performing this procedure on jackknife resampled data sets.[24,25]

IV. RESULTS

We now present the results we obtained in our Monte Carlo simulations that employ the methods presented in the previous section. The 3D compass model was simulated with screw-periodic boundary conditions with $S = 1$ on simple-cubic lattices of sizes $N = L^3$ with $L \in \{8, 12, 16, 20, 24, 28, 32, 36, 40, 44, 48\}$. In each case from 32 to 64 replicas were used in the parallel-tempering scheme. For the smallest lattice inverse temperatures βJ range in $\{4, \ldots, 20\}$, while for the largest lattice βJ was chosen from $\{9.5, \ldots, 11.5\}$. Simulations were performed for at least some 10^7 and up to 3.8×10^7 Monte Carlo sweeps on the largest lattice after an equilibration phase, typically one-tenth of that length.

For all lattice sizes we observe clear indications of a thermal phase transition around $\beta J \approx 10$ in the behavior of the order parameter D, which approaches zero in the high-temperature regime (low β) and a finite value $D > 0$, which characterizes directional ordering, at low temperatures. The two phases are visualized in Fig. 1. Note that up to thermal fluctuations we find all spins in the ordered finite-temperature phase to be aligned with some of the lattice axes even though the ground states of the compass model are not restricted to have such an orientation. Apparently fluctuations around these coaxial configurations are favored through an order-by-disorder mechanism.

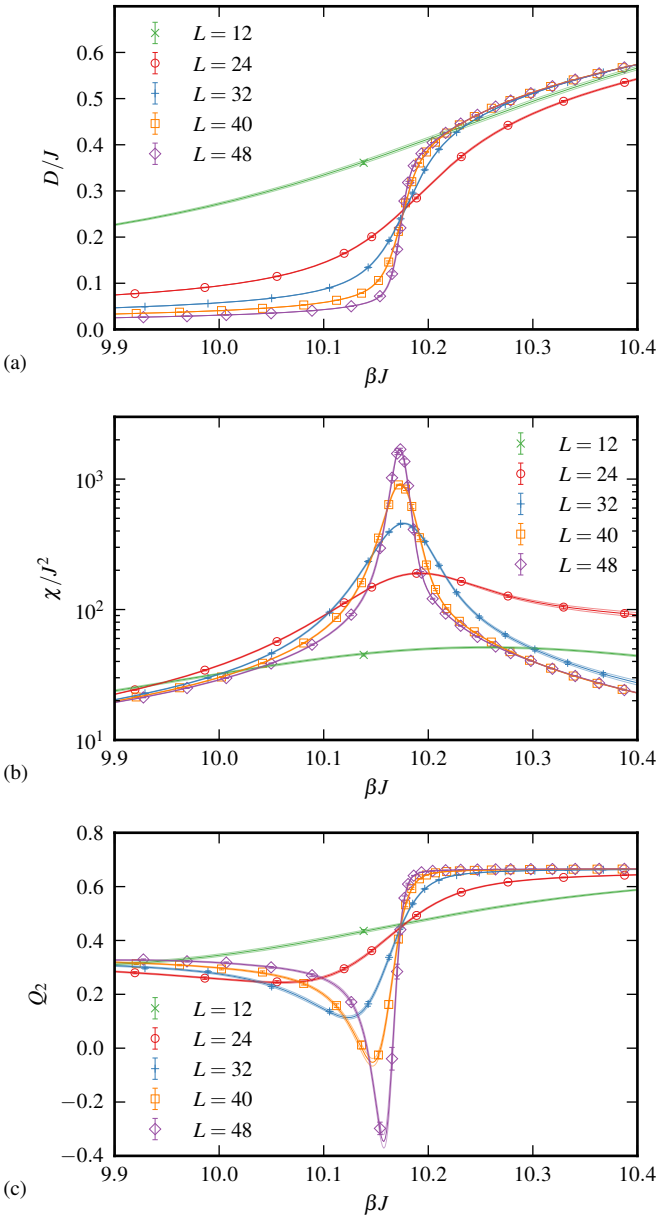

FIG. 2. (Color online) Monte Carlo data for (a) the order parameter D, (b) its susceptibility χ and (c) the Binder parameter Q_2. For clarity the inverse temperature range is limited to a region around the transition point and only selected lattice sizes are included in the plots. Markers with error bars are estimates from single-temperature time series. Continuous lines are from the multiple histogram analysis with faint surrounding lines indicating the 1σ-margin of statistical uncertainty.

In this model with ferromagnetic couplings all spins in one aligned row of an ordered configuration point in the same direction. While the scalar order parameter D describes the degree of this directional ordering and serves to clearly distinguish the phases and identify the transition point, it does not characterize the patterns these rows form in the ordered phase.

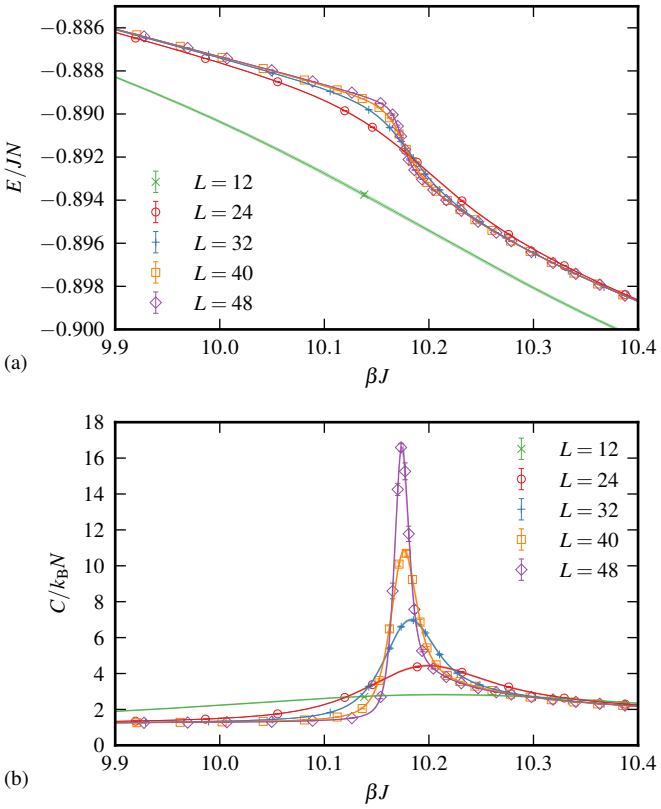

FIG. 3. (Color online) Monte Carlo data for (a) the energy per site E/N and (b) the specific heat capacity C/N. For clarity the inverse temperature range is limited to a region around the transition point and only selected lattice sizes are included in the plots. Markers with error bars are estimates from single-temperature time series. Continuous lines are from the multiple histogram analysis with faint surrounding lines indicating the 1σ-margin of statistical uncertainty.

In this respect it would be interesting to investigate alternative order-parameter definitions discussed in the literature.[1,8,11] Figure 1(b), e.g., shows the formation of a stripe pattern, which, however, is purely an effect of our choice of screw-periodic boundary conditions: All those spins lying in one and the same interconnected loop are forced to point in the same direction. A different choice of the screw parameter S would lead to a different stripe pattern. With periodic boundary conditions directional ordering persists, but the aligned rows will no longer form these visual patterns. It is important to stress that these differences are mere finite-size effects and become meaningless in the thermodynamic limit. Therefore, to clearly characterize the phase transition a careful scaling analysis as presented below in Sec. IV A is very important.

The smoothed jump of the order parameter curve $D(\beta)$ in the temperature region close to the transition point on different lattice sizes can be seen in Fig. 2(a). The transition is accompanied by peaks of the susceptibility χ in Fig. 2(b) and minima of the Binder parameter Q_2 in Fig. 2(c). On the larger lattices also bends in the curves of the normalized energy $E(\beta)/N$ can be seen in the same temperature region in Fig. 3(a) together with peaks of the specific heat capacity $C(\beta)/N$ in Fig. 3(b).

Close to the transition we furthermore find signs for phase coexistence, which is realized in histograms of the order parameter D with two peaks: one corresponding to a more disordered and one to a more ordered phase. By combining our reweighting and optimization algorithms, we can precisely estimate the inverse temperatures $\beta^D_{\mathrm{eqH}}(L)$, where the two peaks of the probability density $P(D)$ have equal height. The estimates for $P(D)$ at all lattice sizes are shown in Fig. 4. The double-peak structure is already present in the smallest system studied here with $L = 8$, but from $L = 16$ to $L = 28$ the relative suppression at the center of the probability distributions successively goes down and up to $L = 24$ the two peaks move closer together. Then, starting from $L = 32$, the behavior changes again: The dip between the two peaks grows with L and also their separation no longer shrinks. Moreover, from $L = 36$ on there are also double-peak structures in the histograms of the energy E. See Fig. 5 for the distributions $P(E)$ measured at the corresponding inverse temperatures $\beta^E_{\mathrm{eqH}}(L)$.

Table I lists the estimated values of $\beta^{\chi}_{\mathrm{max}}(L)$, $\chi_{\mathrm{max}}(L)$, $\beta^C_{\mathrm{max}}(L)$, $C_{\mathrm{max}}(L)/N$, $\beta^{Q_2}_{\mathrm{min}}(L)$, $Q_{2,\mathrm{min}}(L)$, $\beta^D_{\mathrm{eqH}}(L)$ and $\beta^E_{\mathrm{eqH}}(L)$ for all studied lattice sizes L. The signs for phase-coexistence at the transition temperature and the minima of the Binder parameter hint at a first-order phase transition in the thermodynamic limit. In the following we study finite-size scaling relations for the measured quantities to further support or rebut this claim. Even with the application of special screw-periodic boundary conditions finite-size effects appear to be rather severe with an irregular behavior for $L \leq 32$.

A. Transition temperature

With $\beta^C_{\mathrm{max}}(L)$, $\beta^{\chi}_{\mathrm{max}}(L)$, $\beta^{Q_2}_{\mathrm{min}}(L)$, $\beta^D_{\mathrm{eqH}}(L)$ and $\beta^E_{\mathrm{eqH}}(L)$ there are various possible definitions of a lattice-size dependent inverse pseudotransition temperature $\beta^*(L)$. For a discussion of the canonical finite-size scaling at a first-order transition see Ref. 26 and references therein. The inverse pseudotransition temperatures are expected to have a displacement from the true infinite-volume transition point β_0 which to leading order scales proportionally to the reciprocal system size $1/L^3$:

$$\beta^*(L) = \beta_0 + \frac{c^*}{L^3} + \cdots . \tag{10}$$

We test this scaling relation for all definitions of $\beta^*(L)$ given above by performing least-squares fits of Eq. (10) to the $\beta^*(L)$ for various ranges of lattice sizes. The results are given in Table II. Fits of good quality can be made based on all possible definitions with the limitation that we only have very few data points for the histogram-based temperature definitions, where the regular behavior sets in at large lattice sizes. The different estimates of the inverse transition temperature β_0 and their statistical uncertainties are in good agreement with each other. This supports the proposed first-order nature of the transition. The best result is found from the $\beta^C_{\mathrm{max}}(L)$ data, which yields

$$\beta_0 = 10.1700(3)/J \tag{11}$$

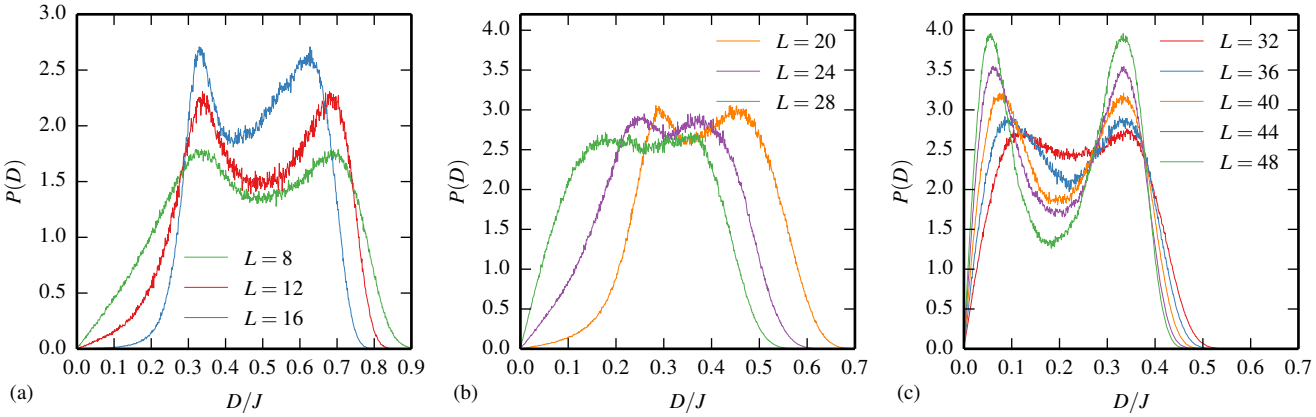

FIG. 4. (Color online) Histograms of the order parameter D for different lattice sizes L at the inverse temperatures $\beta^D_{\mathrm{eqH}}(L)$, where a double-peak structure with equal peak height is obtained. (a) The two peaks hinting at phase coexistence can be made out clearly for small lattices. (b) For medium sized lattices with $L < 32$ the central dip shrinks with growing L. (c) For $L \geq 32$ the suppression between the peaks grows with growing L.

TABLE I. Lattice-size dependent inverse pseudotransition temperatures. Listed are the inverse temperature locations $\beta^{\chi}_{\mathrm{max}}(L)$, $\beta^{C}_{\mathrm{max}}(L)$ and $\beta^{Q_2}_{\mathrm{min}}(L)$ of the extrema of the susceptibility, specific heat and Binder parameter together with the extreme values $\chi_{\mathrm{max}}(L)$, $C_{\mathrm{max}}(L)/N$ and $Q_{2,\mathrm{min}}(L)$ as well as the inverse temperatures $\beta^{D}_{\mathrm{eqH}}(L)$ and $\beta^{E}_{\mathrm{eqH}}(L)$ where the histograms of the order parameter D or the energy E have two peaks of equal height together with the ratios of the estimated probabilities $P_{\mathrm{max}}(L)/P_{\mathrm{min}}(L)$ at the highest peak and at the lowest point in the dip.

L	$\beta^{\chi}_{\mathrm{max}}J$	χ_{max}/J^2	$\beta^{C}_{\mathrm{max}}J$	$C_{\mathrm{max}}/k_{\mathrm{B}}N$	$\beta^{Q_2}_{\mathrm{min}}J$	$Q_{2,\mathrm{min}}/J^2$	$\beta^{D}_{\mathrm{eqH}}J$	$P^{D}_{\mathrm{max}}/P^{D}_{\mathrm{min}}$	$\beta^{E}_{\mathrm{eqH}}J$	$P^{E}_{\mathrm{max}}/P^{E}_{\mathrm{min}}$
8	9.902(4)	20.10(4)	9.834(5)	1.904(3)	8.97(1)	0.230(2)	9.906(4)	1.40(4)		
12	10.26(1)	51(1)	10.21(1)	2.83(3)	9.72(4)	0.297(4)	10.29(1)	1.7(1)		
16	10.42(1)	75(1)	10.246(3)	2.99(2)	9.76(2)	0.293(3)	10.39(1)	1.5(1)		
20	10.205(2)	111(1)	10.208(1)	3.53(2)	9.98(1)	0.272(3)	10.26(1)	1.20(3)		
24	10.192(1)	190(2)	10.199(1)	4.44(3)	10.059(3)	0.244(3)	10.199(3)	1.14(2)		
28	10.180(1)	310(3)	10.188(1)	5.6(1)	10.104(2)	0.17(1)	10.176(1)	1.0(2)		
32	10.177(1)	457(4)	10.183(1)	6.99(5)	10.123(1)	0.11(1)	10.172(1)	1.17(4)		
36	10.176(1)	662(5)	10.180(1)	8.8(1)	10.139(1)	0.05(1)	10.173(1)	1.48(5)	10.177(1)	1.0(1)
40	10.173(1)	916(8)	10.176(1)	10.8(1)	10.147(1)	−0.05(1)	10.1719(5)	1.8(1)	10.175(1)	1.23(2)
44	10.1724(2)	1237(10)	10.1744(3)	13.3(1)	10.1521(4)	−0.17(1)	10.1716(2)	2.1(1)	10.1740(2)	1.47(3)
48	10.1728(4)	1688(26)	10.1742(4)	16.7(2)	10.157(1)	−0.35(2)	10.1727(4)	3.1(2)	10.1744(4)	1.9(1)

for $L \geq 24$ with $\chi^2_{\mathrm{dof}} = 1.12$. This corresponds to a transition temperature

$$T_0 = 0.098328(3) J/k_{\mathrm{B}}. \tag{12}$$

The scaling is also visualized in Fig. 6. While it is possible to consider additional terms with higher powers of $1/L^3$ or exponential corrections[26] in the scaling law (10), this also leads to a higher number of free parameters and in this case does not improve the quality of the fits.

We note that with periodic boundary conditions it may occur that the exponential degeneracy of ground states survives partially also at low, but finite temperatures, leading effectively to a macroscopic degeneracy of distinct ordered states separated from each other by free-energy barriers. This can be understood as a number of ordered phases q that is not constant, but grows exponentially as a function of the system size. It has recently been understood[27,28] that in such a case a modified scaling law

$$\beta^*(L) = \beta_0 + \frac{c^* \ln q}{L^3} + \cdots \tag{13}$$

needs to be applied, which predicts a transmuted leading system-size dependence. An advantage of our choice of screw-periodic boundary conditions is that such degeneracies are mostly lifted. In contrast to the gonihedric plaquette model studied in Refs. 27 and 28 we do not know about any rigorous calculations of this $T > 0$ degeneracy for the 3D compass model with periodic boundary conditions, but assuming a degeneracy $\ln q \propto L^2$ the displacement of $\beta^*(L)$ from the true transition point β_0 would be proportional to $1/L$ rather than to $1/L^3$. Due to very strong finite-size effects we cannot give a full discussion of the asymptotic scaling behavior with periodic boundary conditions at this point. Our (less extensive) data for this case is compatible with the modified ansatz, but does not allow to discriminate between the two options. We have also checked modified scaling relations corresponding to

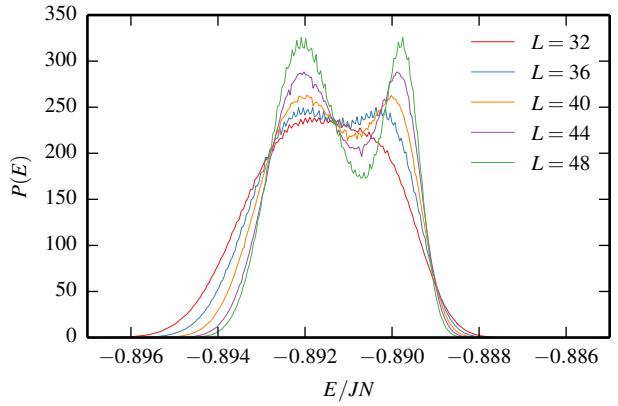

FIG. 5. (Color online) Histograms of the energy per site E/N for various lattice sizes L at the inverse temperatures $\beta^E_{\mathrm{eqH}}(L)$, where a double-peak structure with equal peak height is obtained for $L > 32$. For $L = 32$ and smaller lattices no double-peak distribution can be found at any temperature. The $L = 32$ histogram in the plot is shown only for comparison and is taken at a temperature close to that of the others.

$\ln q \propto L^2$ and $\ln q \propto L$ for the case of screw-periodic boundary conditions and have found here no compelling numerical evidence against the conventional $1/L^3$ law as reported above.

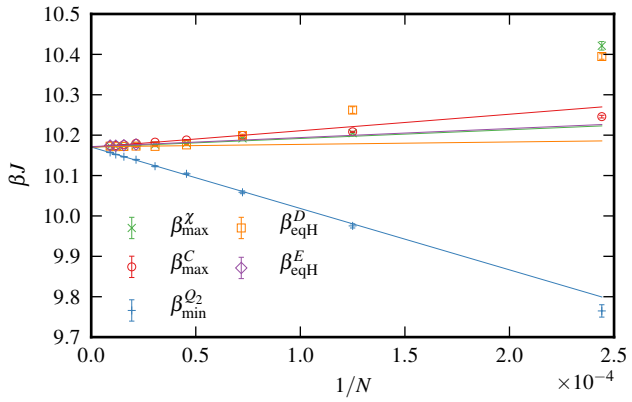

FIG. 6. (Color online) Finite-size scaling of inverse pseudotransition temperatures from Table I for $L \geq 16$ together with the best fits from Table II, which allow to extrapolate the infinite-volume transition point β_0.

B. Interface tension

On lattices of size L^3 the suppression of the minimum between the two peaks of the probability distribution of the energy or the order parameter at a first-order phase transition is expected to grow exponentially with L^2:

$$P_{\mathrm{max}}(L)/P_{\mathrm{min}}(L) \propto \mathrm{e}^{2\beta\sigma L^2}. \tag{14}$$

Configurations corresponding to $P_{\mathrm{min}}(L)$ are in a mixture of the ordered and the disordered phases with interfaces that

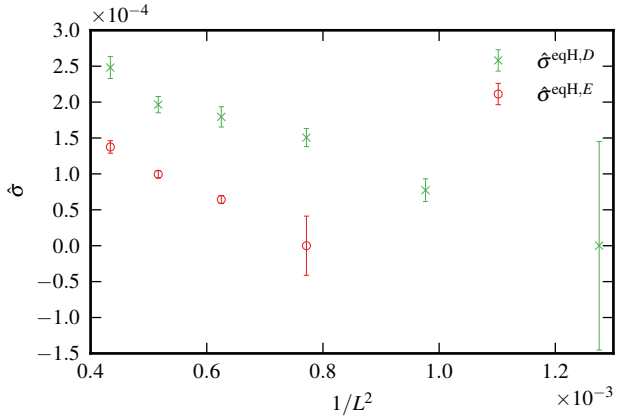

FIG. 7. (Color online) Reduced interface tensions $\hat{\sigma}(L)$ calculated from $P(D)$ histograms at $\beta^D_{\mathrm{eqH}}(L)$ and from $P(E)$ histograms at $\beta^E_{\mathrm{eqH}}(L)$ plotted over $1/L^2$ for $L \geq 28$.

contribute an excess free energy of $2\sigma L^2$, where the free-energy density σ is the interface tension.[26] We compute lattice size dependent estimates of the reduced interface tension $\hat{\sigma}(L) = \beta\sigma(L)$ from the double-peaked probability distributions $P(D)$ at $\beta^D_{\mathrm{eqH}}(L)$ or $P(E)$ at $\beta^E_{\mathrm{eqH}}(L)$ with the relation

$$\hat{\sigma}(L) = \frac{1}{2L^2} \ln\left[\frac{P_{\mathrm{max}}(L)}{P_{\mathrm{min}}(L)}\right], \tag{15}$$

where $P_{\mathrm{max}}(L)/P_{\mathrm{min}}(L)$ is the ratio of the estimated probabilities in the peak and in the dip as taken from Table I. In Fig. 7 the results are plotted over $1/L^2$ for $L \geq 28$, which excludes the irregular behavior for the small lattices. While the reduced interface tension does not yet reach its asymptotic constant value on the lattice sizes studied here, $\hat{\sigma}(L)$ grows with L and does not appear to vanish in the limit of large systems, which otherwise would be an argument against the first-order nature of the transition. From the available data an approximate infinite-volume value of $\hat{\sigma} \approx 3\times10^{-4}$ can be anticipated.

V. SUMMARY AND CONCLUSIONS

In this paper we have presented an extensive Monte Carlo investigation of the classical compass model on the simple-cubic lattice. Our results show that directional ordering is present in a low-temperature phase, which is reached via a thermal first-order transition from a disordered high-temperature phase. By a detailed finite-size scaling analysis we could determine a precise estimate of the transition temperature $T_0 = 0.098328(3)J/k_{\mathrm{B}}$. This value agrees with the one mentioned in an earlier publication,[29] but the high-temperature series expansions presented in Ref. 14 could not identify this phase transition. First-order transitions are generally difficult to detect by these techniques, in particular when no low-temperature series are available.

The recently discovered (and for the gonihedric plaquette model numerically confirmed) influence of a macroscopic degeneracy of the low-temperature phases on the leading finite-

TABLE II. Results of least-squares fits of the inverse pseudotransition temperatures $\beta^*(L)$ taken from Table I to estimate the infinite-volume transition point β_0 by relations of the form $\beta^*(L) = \beta_0 + c^*/L^3$. Here n is the number of included data points ranging from the smallest considered lattice size $L_{\min}$ up to the largest $L_{\max} = 48$. $\chi^2_{\text{dof}} = \chi^2/(n-2)$ is a measure to help with the estimation of the validity of the fit. The best fits are marked bold for each type of pseudotransition temperature.

$L_{\min}$	n	$\beta^{\chi}_{\max,0}J$	χ^2_{dof}	$\beta^{C}_{\max,0}J$	χ^2_{dof}	$\beta^{Q_2}_{\min,0}J$	χ^2_{dof}	$\beta^{D}_{\text{eqH},0}J$	χ^2_{dof}	$\beta^{E}_{\text{eqH},0}J$	χ^2_{dof}
8	11	10.176(3)	268.62	10.180(4)	445.25	10.157(4)	148.63	10.174(3)	259.64		
12	10	10.170(2)	51.07	10.173(2)	62.05	10.170(2)	14.69	10.168(2)	86.60		
16	9	10.169(2)	42.43	10.171(1)	6.85	10.171(1)	1.97	10.165(3)	78.28		
20	**8**	10.1693(5)	3.52	10.171(1)	7.15	**10.171(1)**	**1.57**	10.169(2)	22.40		
24	**7**	10.169(1)	4.18	**10.1700(3)**	**1.12**	10.170(1)	1.57	10.170(1)	12.28		
28	**6**	**10.1702(5)**	**1.60**	10.1699(5)	1.38	10.170(1)	1.59	**10.171(1)**	**2.85**		
32	5	10.170(1)	2.10	10.170(1)	1.64	10.170(1)	1.79	10.172(1)	2.64		
36	**4**	10.170(1)	3.11	10.169(1)	2.34	10.170(1)	2.02	10.172(1)	3.95	**10.172(1)**	**2.84**
40	3	10.172(2)	2.66	10.171(2)	2.16	10.171(2)	1.80	10.173(2)	4.51	10.173(2)	3.22

size scaling behavior of first-order phase transitions[27,28] renews the interest in a precise characterization of the ground-state and low-temperature degeneracies of the compass model. A rigorous treatment along the lines of Refs. 30–32 for the closely related 120° model and the gonihedric model is beyond the scope of the present paper focusing on an accurate determination of the first-order character of the phase transition, but would certainly be a worthwhile project for future studies, especially with a view on the "order-by-disorder" mechanism.

Due to the negative-sign problem, quantum Monte Carlo simulations of the 3D compass model are out of reach. However, while additional quantum fluctuations may destroy directional ordering at low temperatures in the quantum model, from Ginzburg-Landau theory one generally expects the nature of the phase transition to be the same in the quantum model as in the classical model. Symmetry considerations for the nematic-like type of order parameter of the t_{2g} compass model support the expectation of a continuous transition in 2D and a first-order transition in 3D, just as observed in the Monte Carlo simulations. Taken together, we firmly anticipate a first-order phase transition to occur also in the quantum compass model and look forward to experimental studies of directional ordering in non-low dimensional samples.

ACKNOWLEDGMENTS

We thank C. Hamer, J. Oitmaa and W. Selke for useful discussions initiating this work, as well as A. Rosch and S. Trebst for further helpful conversations. Partial support by the Deutsche Forschungsgemeinschaft (DFG) through Graduate School GSC185 "BuildMoNa" and the Deutsch-Französische Hochschule (DFH-UFA) through the binational German-French Graduate School under grant number CDFA-02-07 is gratefully acknowledged. M.G. thanks the Bonn-Cologne Graduate School of Physics and Astronomy (BCGS) for support.

* gerlach@thp.uni-koeln.de
† janke@itp.uni-leipzig.de; http://www.physik.uni-leipzig.de/cqt.html

[1] For a comprehensive recent review of the compass and related Kitaev models, see Z. Nussinov and J. van den Brink, arXiv:1303.5922 [cond-mat.str-el].
[2] K. I. Kugel and D. I. Khomskii, Sov. Phys. Usp. **25**, 231 (1982).
[3] J. van den Brink, New J. Phys. **6**, 201 (2004).
[4] B. Douçot, M. Feigel'man, L. Ioffe, and A. S. Ioselevich, Phys. Rev. B **71**, 024505 (2005).
[5] P. Milman, W. Maineult, S. Guibal, L. Guidoni, B. Douçot, L. Ioffe, and T. Coudreau, Phys. Rev. Lett. **99**, 020503 (2007).
[6] S. Gladchenko, D. Olaya, E. Dupont-Ferrier, B. Douçot, L. B. Ioffe, and M. E. Gershenson, Nat. Phys. **5**, 48 (2009).
[7] C. Batista and Z. Nussinov, Phys. Rev. B **72**, 045137 (2005).
[8] Z. Nussinov and E. Fradkin, Phys. Rev. B **71**, 195120 (2005).
[9] J. Villain, R. Bidaux, J.-P. Carton, and R. Conte, J. Phys. (Paris) **41**, 1263 (1980).
[10] C. L. Henley, Phys. Rev. Lett. **62**, 2056 (1989).
[11] A. Mishra, M. Ma, F.-C. Zhang, S. Guertler, L.-H. Tang, and S. Wan, Phys. Rev. Lett. **93**, 207201 (2004).
[12] S. Wenzel and W. Janke, Phys. Rev. B **78**, 064402 (2008).
[13] S. Wenzel, W. Janke, and A. M. Läuchli, Phys. Rev. E **81**, 066702 (2010).
[14] J. Oitmaa and C. Hamer, Phys. Rev. B **83**, 094437 (2011).
[15] E. Bittner, A. Nußbaumer, and W. Janke, Nucl. Phys. B **820**, 694 (2009).
[16] N. Metropolis, A. W. Rosenbluth, M. N. Rosenbluth, A. H. Teller, and E. Teller, J. Chem. Phys. **21**, 1087 (1953).
[17] U. Wolff, Phys. Rev. Lett. **62**, 361 (1989).
[18] C. J. Geyer, in *Computing Science and Statistics: Proceedings of the 23rd Symposium on the Interface*, edited by E. M. Keramidas (Interface Foundation, Fairfax Station, 1991), pp. 156–163.
[19] K. Hukushima and K. Nemoto, J. Phys. Soc. Jpn. **65**, 1604 (1996).
[20] D. Sabo, M. Meuwly, D. L. Freeman, and J. D. Doll, J. Chem. Phys. **128**, 174109 (2008).
[21] A. M. Ferrenberg and R. H. Swendsen, Phys. Rev. Lett. **63**, 1195 (1989).
[22] J. D. Chodera, W. C. Swope, J. W. Pitera, C. Seok, and K. A. Dill, J. Chem. Theory Comput. **3**, 26 (2007).

[23] R. P. Brent, *Algorithms for Minimization Without Derivatives* (Prentice-Hall, Englewood Cliffs, 1973), Chap. 5.
[24] B. Efron, *The Jackknife, the Bootstrap and Other Resampling Plans* (SIAM, Philadelphia, 1982).
[25] W. Janke, in *Computational Many-Particle Physics*, Lect. Notes Phys., Vol. 739, edited by H. Fehske, R. Schneider, and A. Weiße (Springer-Verlag, Berlin, 2008), pp. 79–140.
[26] W. Janke, in *Computer Simulations of Surfaces and Interfaces*, NATO Science Series II: Mathematics, Physics and Chemistry, Vol. 114, edited by B. Dünweg, D. P. Landau, and A. I. Milchev (Kluwer Academic Publishers, Dordrecht, 2003), pp. 111–135.
[27] M. Mueller, W. Janke, and D. A. Johnston, Phys. Rev. Lett. **112**, 200601 (2014).
[28] M. Mueller, D. A. Johnston, and W. Janke, Nucl. Phys. B **888**, 214 (2014).
[29] S. Wenzel and A. M. Läuchli, Phys. Rev. Lett. **106**, 197201 (2011).
[30] Z. Nussinov, M. Biskup, L. Chayes, and J. van den Brink, Europhys. Lett. **67**, 990 (2004).
[31] R. Pietig and F. J. Wegner, Nucl. Phys. B **466**, 513 (1996).
[32] R. Pietig and F. J. Wegner, Nucl. Phys. B **525**, 549 (1998).